Production and Decay of HF in ATLAS

Angel Campoverde[*][†]

University of Siegen
E-mail: angel.campoverde@cern.ch

An angular analysis of the decay of $B_d \to K^* \mu^+ \mu^-$ is peformed for a number of angular coefficients, which are measured as a function of the invariant mass squared of the dimuon system for data collected at $\sqrt{s} = 8$ TeV by ATLAS [2], at the LHC [1]. Comparisons are made to theoretical predictions, including for the observable P_5', for which there has been recent tension between theory and experiment. In addition a study of kinematical correlations in B hadron pair production is presented.

---

[*]Speaker.

1. Angular analysis of $B_d \rightarrow K^* \mu^+ \mu^-$ decays in pp collisions at $\sqrt{s} = 8$ TeV with the ATLAS detector

The $B_d \rightarrow K^* \mu^+ \mu^-$ decay is relevant because it involves Flavour Changing Neutral Currents (FCNC) in the $\bar{b} \rightarrow \bar{s} \mu^+ \mu^-$ transition. Therefore it is strongly supressed at tree level and only higher order Feynman diagrams contribute; figure 1a shows one of those processes.
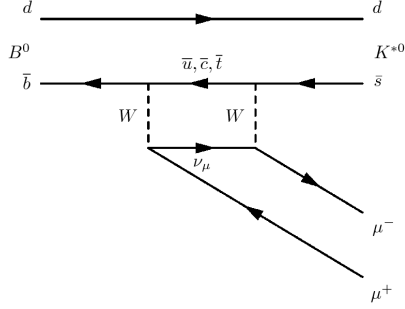
(a) The diagram above shows a process allowed by the SM, that contributes to the $B_d \rightarrow K^* \mu^+ \mu^-$ yield.
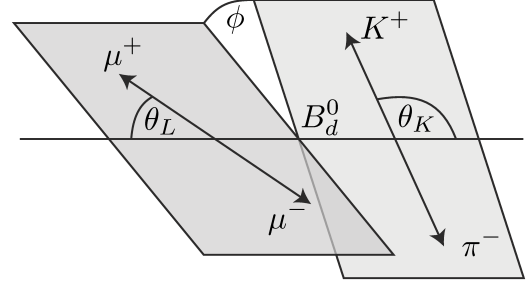
(b) The diagram above shows the definitions of the angles in the $B_d \rightarrow K^* \mu^+ \mu^-$ decay.

Figure 1: Figures taken from [3].

The goal of this analysis [3] is to measure angular distributions associated to the $B_d \rightarrow K^* \mu^+ \mu^-$ decay. These distributions are parametrized by F_L, the fraction of longitudinally polarized $K(892)^*$ mesons (from now on referred as K^*), and the parameters S_3, S_4, S_5, ... ,S_9.
LHCb has studied this decay and found discrepancies between data and SM predictions with a 3.4σ significance [5]; this is another reason why this particular decay is of interest. CMS has performed this study as well [6].

1.1 Analysis Description

The data used to perform this measurement are 20.3 fb^{-1} of proton-proton collisions collected by the ATLAS detector in 2012. The $B_d \rightarrow K^* \mu^+ \mu^-$ decays are parametrized by three angles and the mass of the system as shown in figure 1b.
In the diagram θ_L is evaluated in the center of mass of the dimuon system; θ_K, in the center of mass of the K^+ and π^- mesons and ϕ in the center of mass of the B meson. The analysis is performed in different bins of the dimuon invariant mass q^2.
The angular dependence of the differential cross-section associated to the P-wave can be seen in equation 1.1, where all the angular parameters already mentioned are used.

$$\frac{1}{d\Gamma/dq^2} \frac{d^4\Gamma}{d\cos\theta_L d\cos\theta_K d\phi dq^2} = \frac{9}{32\pi} \left[\frac{3(1-F_L)}{4} \sin^2\theta_K + F_L \cos^2\theta_K + \frac{1-F_L}{4} \sin^2\theta_K \cos 2\theta_L \right.$$
$$- F_L \cos^2\theta_K \cos 2\theta_L + S_3 \sin^2\theta_K \sin^2\theta_L \cos 2\phi + S_4 \sin 2\theta_K \sin 2\theta_L \cos\phi + S_5 \sin 2\theta_K \sin\theta_L \cos\phi$$
$$\left. + S_6 \sin^2\theta_K \cos\theta_L + S_7 \sin 2\theta_K \sin\theta_L \sin\phi + S_8 \sin 2\theta_K \sin 2\theta_L \sin\phi + S_9 \sin^2\theta_K \sin^2\theta_L \sin 2\phi \right]$$

$$(1.1)$$

There are large uncertainties associated to the form factors; in order to mitigate them a new parametrization $S_i \rightarrow P_i$ is chosen. However, due to low statistics, it is still not possible to use this parametrization. Additionally, a set of four trigonometric transformations, from now on called *folding schemes*, is used. Thus, the final set of P_i' parameters is obtained.

Each of the folding schemes is applied separately to the data, resulting in four datasets, any of them can be used to extract F_L and S_3. Nevertheless, it is not possible to extract anymore S_6 and S_9. The former parameter is related to the forward-backward asymmetry through $A_{FB} = 3S_6/4$.

1.2 Event Selection

An event needs to trigger algorithms that look for events with one, two or three muons; this requirement selects 29% of the signal events. The dimuon system is required to be consistent with having originated from a common vertex. The K^* meson is built from two tracks with opposite charge, while the B_d^0 meson is formed by four tracks and is required to be displaced from the interaction vertex. Given that ATLAS cannot distinguish between kaons and pions, requirements are imposed on the $K\pi$ system's mass to tag the meson as B_d^0 or $\bar{B}_d^0$. When multiple candidates are found in an event, the one with the smallest $|m_{K\pi} - m_{K^*}|/\sigma(m_{K\pi})$ is kept. The mistagging is also reduced by retaining the B meson with the smallest B vertex fit χ^2.

The dimuon invariant mass is also used to define two control regions; where the two muons originate from the decay of a J/ψ, in $q^2 \in [8, 11]$ GeV and where they come from the decay of a $\psi(2S)$, in $q^2 \in [12, 15]$ GeV. Contributions from $\phi(1020)$ are excluded by removing any candidate with $q^2 \in [0.98, 1.1]$ GeV^2. Otherwise, the signal region encompasses $q^2 \in [4m_\mu^2, 6$ GeV$]$, excluding anything above to avoid the charmonium low mass tail contamination.

1.3 Analysis

Once the events in data have been selected, they are fitted to PDFs representing the background and the signal components. The mass distribution of the background is modelled by an exponential PDF, while the angular dependence is modelled by second order Chebyshev polynomials in $\cos(\theta_L)$, $\cos(\theta_K)$ and ϕ. Any disagreements associated to the choice of PDFs is accounted for as systematics.

The signal's mass depencence is modelled with a modified Gaussian PDF with mean m_0 and width $\xi\sigma$, where σ is the error on the mass of the B candidate, while m_0 and ξ are extracted from fits to the control regions mentioned above. The angular dependence is taken as the decay amplitude of the P-wave (see 1.1) after a given folding scheme is applied. The angular dependence of the acceptance is modelled also by polynomials in the angles and is extracted from simulated samples.

1.4 Results

The measured angular parameters are consistent with the Standard Model expectations. Figure 2 shows that P_4' and P_5' are 2.7σ away from the prediction of Descotes-Genon et al. (DHMV) [7] in the $q^2 \in [4, 6]$ GeV bin; while P_8' shows a small disagreement in the $q^2 \in [2, 4]$ GeV bin. This is also consistent with what LHCb observed.
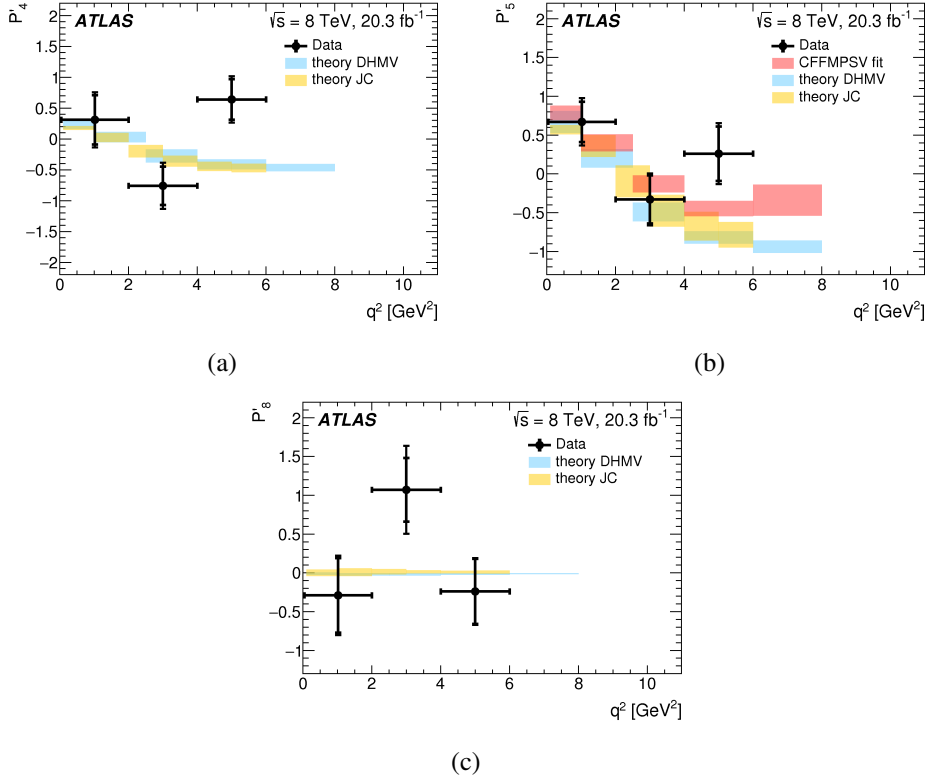
(a)

(b)

(c)

Figure 2: The three figures represent the comparison between data and different theory predictions for P'_4, P'_5 and P'_8. Figures taken from [3].

2. Measurement of b-hadron pair production with the ATLAS detector

The goal of this analysis [4] is to measure the differential cross-section for $b\bar{b}$ production down to zero opening angle. Constraining the theoretical estimates of this cross-section is important because $g \to b\bar{b}$ is the main source of background for the $h \to b\bar{b}$ Higgs decay. Furthermore, as the LHC center of mass energy increases, the Higgs boson becomes more boosted, giving rise to smaller angles between the b and $\bar{b}$ quarks.

2.1 Analysis Description

The strategy of this analysis is to measure the first b quark through the $J/\psi \to \mu^+\mu^-$ decay, where the J/ψ meson originates from a B meson directly or through some $c\bar{c}$ excited state. The second b quark is measured through the muon in the semileptonic decay $b \to c \to \mu + X$. The cross-section is binned in several observables like $\Delta R(J/\psi, \mu)$, $\Delta y(J/\psi, \mu)$, $p_T(J/\psi, \mu)$, among others.

2.2 Event Selection

This analysis uses 11.4 fb^{-1} of proton proton collisions collected by ATLAS in 2012 at $\sqrt{s} = 8$ TeV. These events are required to trigger an algorithm designed to recognize two muons originating from a J/ψ meson. The muons are built by combining Inner Detector tracks with Muon

Spectrometer segments and are required to satisfy standard quality criteria. The reconstructed J/ψ is required to be formed from two oppositely charged muons, geometrically matched to the muons built by the trigger algorithms. The third muon is taken as the one with the highest p_T that was not used to build the J/ψ meson.

2.3 Analysis

In order to estimate the fiducial yield of events containing a $J/\psi \to \mu^+\mu^-$ decay, one has to apply corrections to compensate for trigger and muon reconstruction inefficiencies. Apart from the combinatorial background, associated to the *fake J/ψ background*, there are two components present in data, one with J/ψ mesons originating from the primary interaction, known as *prompt* and another, originating from the decay of *B* mesons, known as *non-prompt*. In order to separate the prompt, non-prompt and fake J/ψ contributions, a 2D fit is used, whose projections in the J/ψ mass and lifetime are shown in figure 3. The second ingredient, the yield of events with
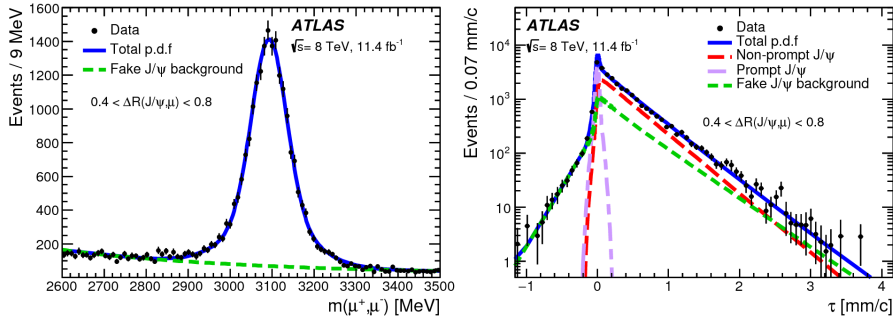

Figure 3: Projection of 2D fit to J/ψ candidates in data. Figures taken from [4].

a $J/\psi \to \mu^+\mu^-$ decay *and* a third non-prompt muon, is obtained also with a 2D fit. In order to remove the contribution of prompt J/ψ decays, and thus increase the proportion of signal, a requirement of $\tau > 0.25$ mm/c is applied to the J/ψ. The fake J/ψ yield from the previous fit is used to constrain the fake J/ψ component, while the other background components are estimated from data as shown in figure 4. In this case, the discriminating variables are a BDT score, used to
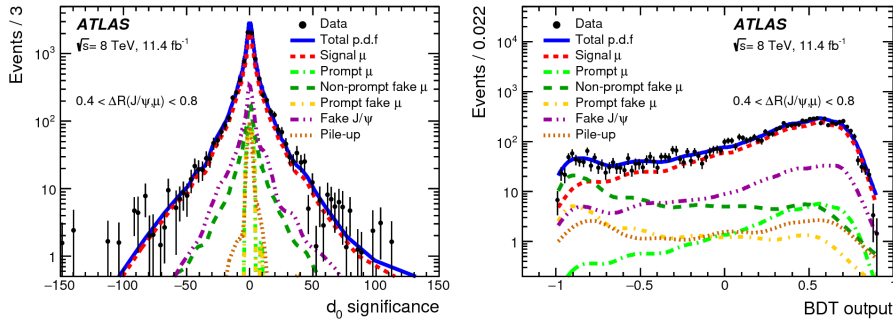

Figure 4: 2D fit to muons to data. The left plot shows the projection in the S_{d0}, the right plot shows the fit in the BDT score. Figures taken from [4].

distinguish fake from true muons and the d_0 significance, which discriminates between prompt and non-prompt muons.

2.4 Results

The measured fiducial cross-section is $17.7 \pm 0.1(\text{stat}) \pm 2.0(\text{syst})$ nb. Due to the lack of accuracy of the leading order calculations used to produce the simulated samples, the comparison with the theoretical expectation is done using the *normalized* differential cross-section, instead of the differential cross-section. Figure 5 shows the predictions of several generators and data for two regimes in p_T.
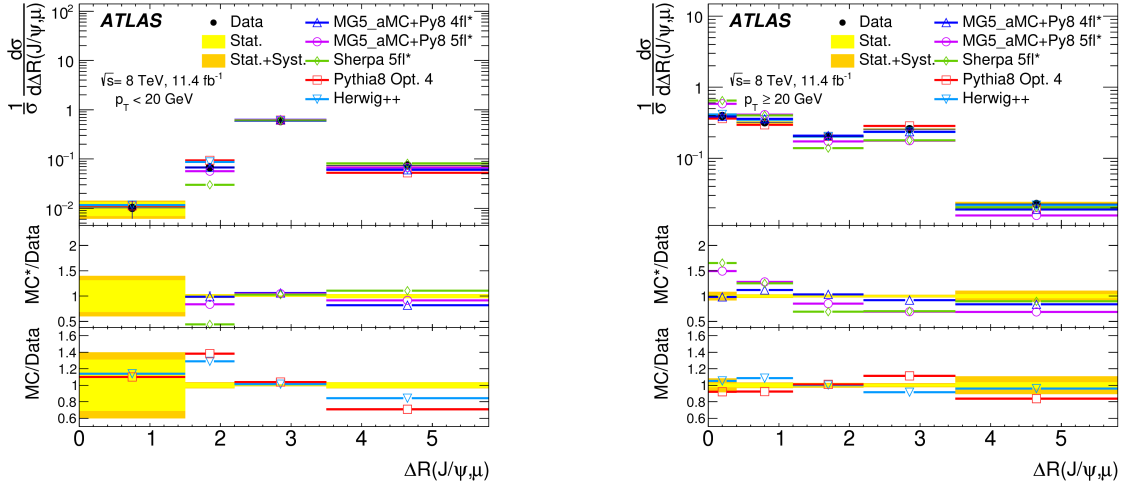

Figure 5: Comparison of differential cross-sections in data and simulation, for $p_T < 20$ GeV (left) and $p_T \geq 20$ GeV (right). Figures taken from [4].

References

[1] L. Evans and P. Bryant, *LHC Machine*, 2008 JINST 3 S08001.

[2] ATLAS Collaboration, *The ATLAS Experiment at the CERN Large Hadron Collider*, 2008 JINST 3 S08003.

[3] ATLAS Collaboration, *Angular analysis of $B_d^0 \to K^* \mu^+ \mu^-$ decays in pp collisions at $\sqrt{s} = 8$ TeV with the ATLAS detector*, CERN-EP-2017-161 [hep-ex/1805.04000].

[4] ATLAS Collaboration, *Measurement of b-hadron pair production with the ATLAS detector in proton-proton collisions at $\sqrt{s} = 8$ TeV*, JHEP 11 (2017) 62 [hep-ex/1705.03374v2]

[5] LHCb Collaboration, *Angular analysis of the $B^0 \to K^* \mu^+ \mu^-$ decay using 3fb^{-1} of integrated luminosity*, JHEP 02 (2016) 104 [hep-ex/1512.04442]

[6] CMS Collaboration, *Measurement of angular parameters from the decay $B^0 \to K^{*0} \mu^+ \mu^-$ in proton-proton collisions at $\sqrt{s} = 8$ TeV*, Phys. Lett. B 781 (2018) 517 [hep-ex/1710.02846]

[7] S. Descotes-Genon, L. Hofer, J. Matias and J. Virto, *On the impact of power corrections in the prediction of $B_d \to K^* \mu^+ \mu^-$ observables*, JHEP 12 (2014) 125.